Supplementary Information

For

One-Step Instant Synthesis of Protein-Conjugated Quantum Dots at Room Temperature

Xuewen He, Li Gao, and Nan Ma*

The Key Lab of Health Chemistry and Molecular Diagnosis of Suzhou, College of Chemistry, Chemical Engineering and Materials Science

Soochow University, Suzhou, 215123, P. R. China

Correspondence should be addressed to N.M. (nan.ma@suda.edu.cn)

Table of Contents

Index of Supplemental Figures and Tables

1. Optical characterization of QDs

1.1 Absorption spectra and photoluminescence spectra of $Zn_xHg_{1-x}Se$ QDs synthesized with different Hg/Zn precursor ratios.

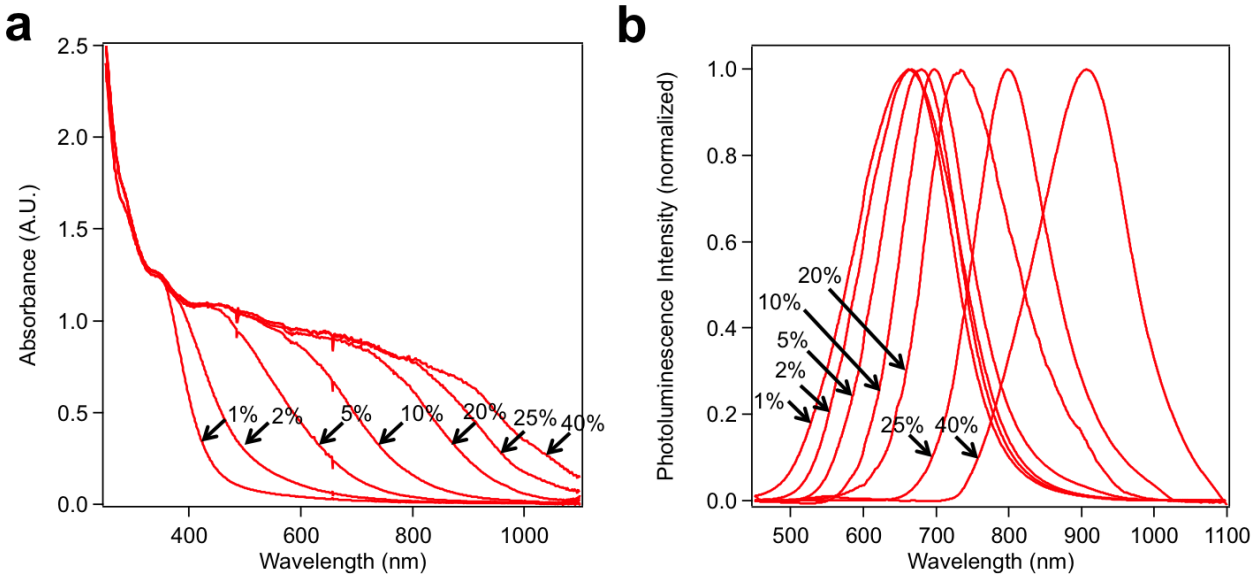

Figure S1. Absorption spectra (a) and photoluminescence spectra (b) of MPA-capped $Zn_xHg_{1-x}Se$ QDs synthesized at different Hg/Zn precursor ratios (1%, 2%, 5%, 10%, 20%, 25%, 40%).

1.2 Absorption spectra and photoluminescence spectra of $Zn_xHg_{1-x}Se$ QDs synthesized with only BSA or BSA/MPA.

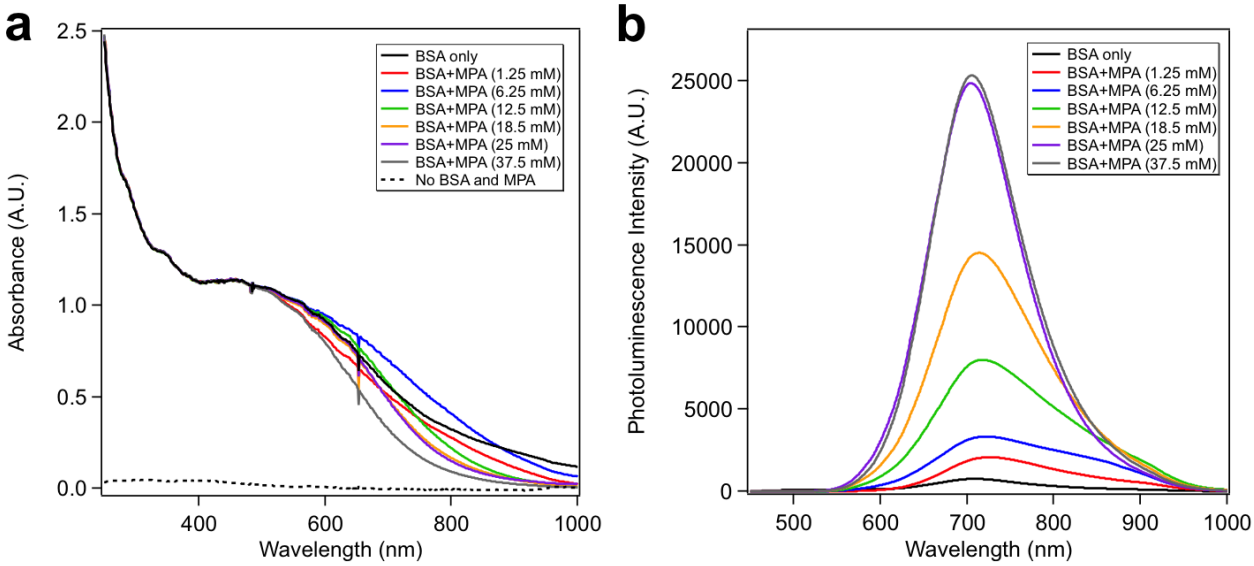

Figure S2. Absorption spectra (a) and photoluminescence spectra (b) of $Zn_xHg_{1-x}Se$ QDs synthesized with BSA (5.0 mg/mL) and different concentrations of MPA (0, 1.25, 6.25, 12.5, 18.5, 25, 37.5 mM). The dashed line in (a) is the absorption spectrum of the product synthesized without BSA and MPA.

2. Nanocharacterization of QDs

2.1 Analysis of the structure of $Zn_xHg_{1-x}Se$ QDs

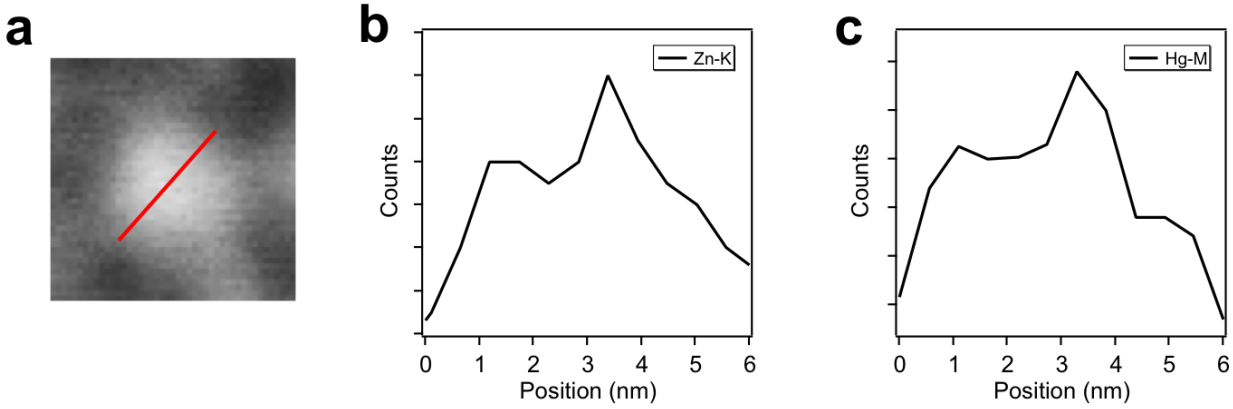

Figure S3. An EELS line scan of a single $Zn_xHg_{1-x}Se$ QD (Hg/Zn precursor ratio = 10%). (a) STEM HAADF image of the $Zn_xHg_{1-x}Se$ QD and the position of the line scan (red line) ; (b) EELS signal intensity of Zn across the diameter of the particle; (c) EELS signal intensity of Hg across the diameter of the particle. There is a similar distribution pattern of the Zn element and the Hg element across the diameter of a single $Zn_xHg_{1-x}Se$ QD, revealing that the QD possesses an alloy structure rather than a core-shell structure.

In the paper by *AM Smith et al.* (*J. Am. Chem. Soc.* **2011**, *133*, 24-26) the authors synthesized a type of $Hg_xCd_{1-x}Te$ alloyed QDs in organic phase via cation exchange. They found that the homogeneous alloyed $Hg_xCd_{1-x}Te$ QDs have an obvious absorption peak whereas the inhomogeneous alloyed $Hg_xCd_{1-x}Te$ QDs have a broad absorption spectrum without an obvious absorption peak. In our study we found that the $Zn_xHg_{1-x}Se$ QDs have a broad absorption spectrum without an obvious absorption peak, which is quite analogous to the inhomogeneous alloyed QDs in the *JACS* paper. Since the as-prepared $Zn_xHg_{1-x}Se$ QDs possess a narrow size distribution, the broad absorption spectrum of these QDs is mainly attributed to the inhomogeneous alloyed structure.

2.2 TEM images of $Zn_xHg_{1-x}Se$ QDs synthesized with only BSA

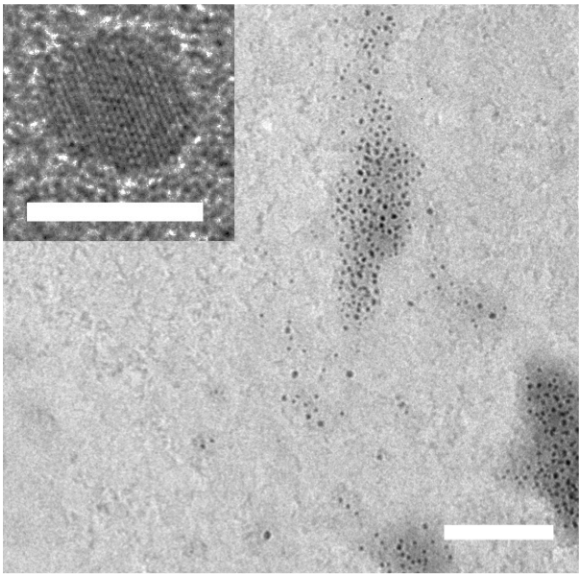

Figure S4. TEM image of $Zn_xHg_{1-x}Se$ QDs synthesized with only BSA. The inset depicts the high-resolution TEM image of a single QD. The scale bars are 50 nm in low magnification image and 5 nm in high-resolution image.

2.3 TEM images of $Zn_xHg_{1-x}Se$ QDs synthesized with only peptide

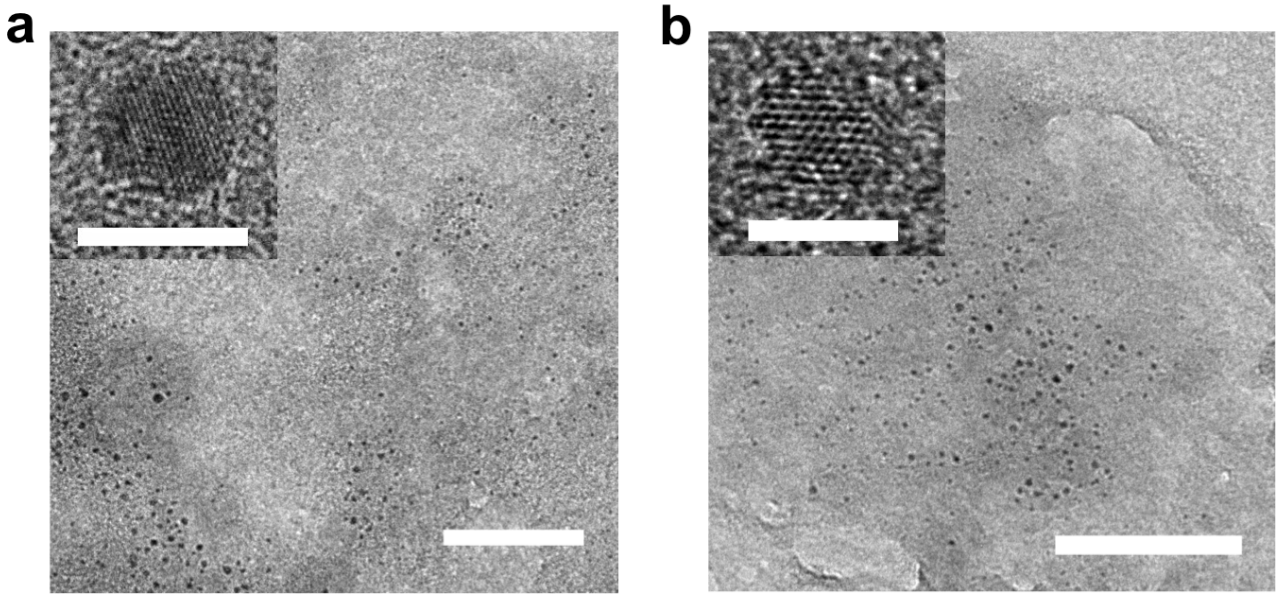

Figure S5. TEM image of $Zn_xHg_{1-x}Se$ QDs synthesized with only peptide (a) HHHHHHCGKRK and (b) HHHHHH. The inset depicts the high-resolution TEM image of a single QD. The scale bars are 50 nm in low magnification image and 5 nm in high-resolution image.

2.4 Protein standards for gel filtration chromatography sizing

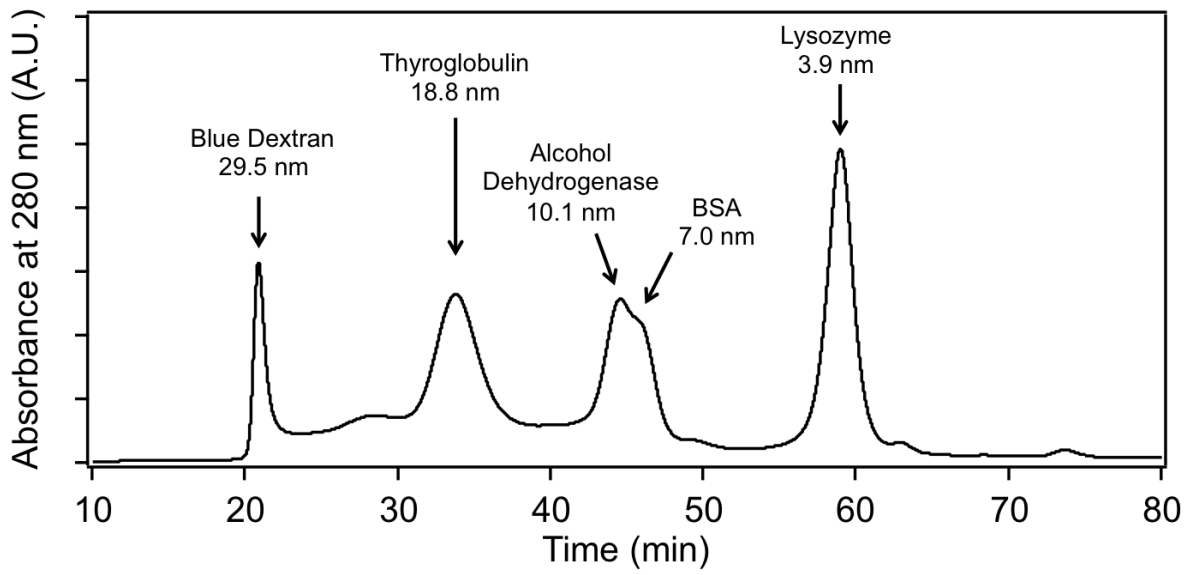

Figure S6. Protein standards for gel filtration chromatography sizing.

2.5 DLS measurements of BSA-QDs and MPA-QDs

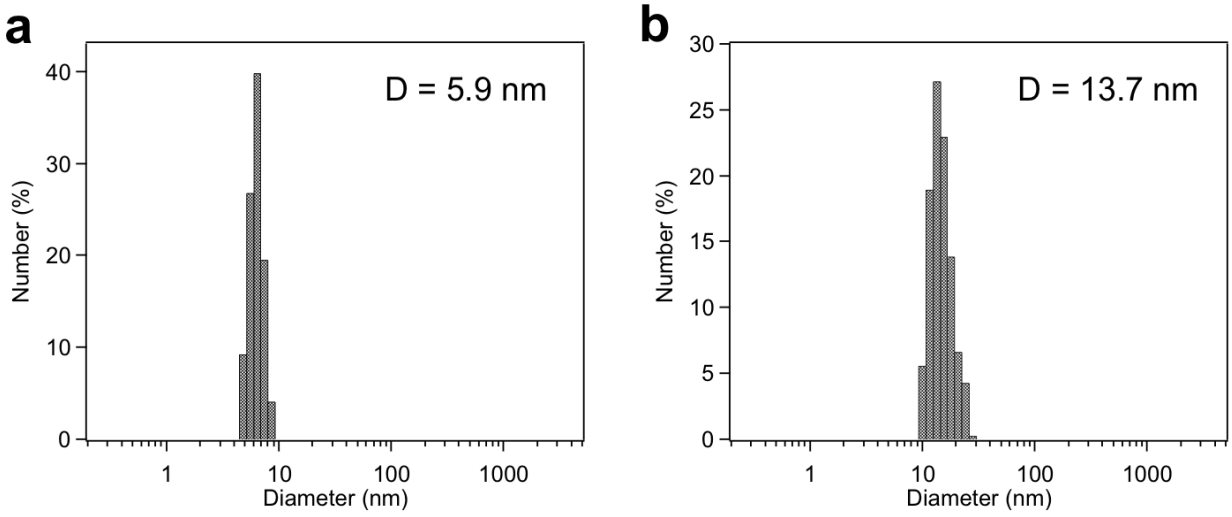

Figure S7. Hydrodynamic diameters of MPA-QDs and BSA-QDs measured by DLS. (a) MPA-QDs (b) BSA-QDs.

3. Stability measurements of QDs

3.1 Colloidal stability of BSA-QDs and MPA-QDs

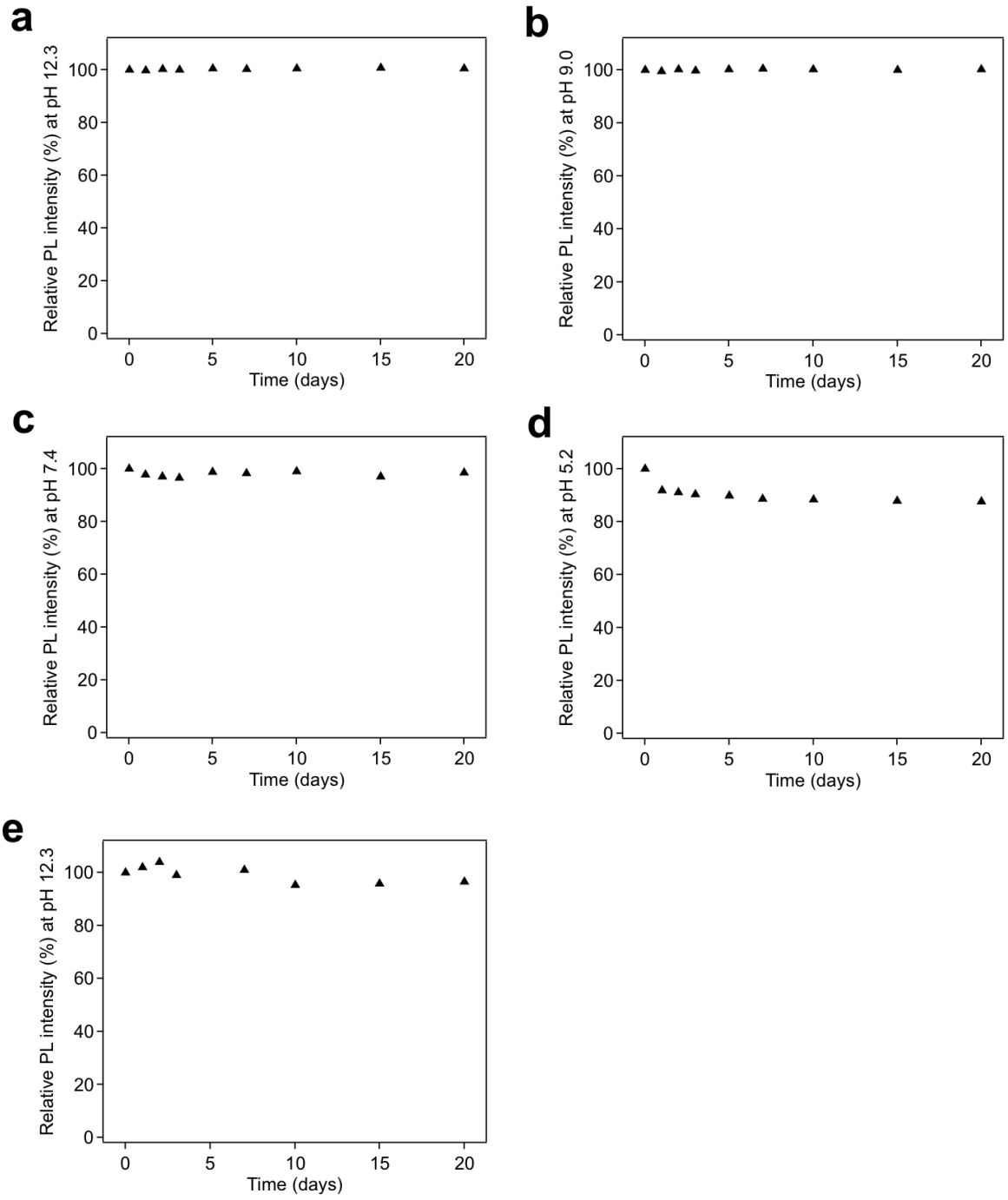

Figure S8. (a)-(d) Relative photoluminescence intensities (at 700 nm) of BSA-QDs stored at different pHs for 0, 1, 2, 3, 5, 7, 10, 15, 20 days ((a) pH 12.3; (b) pH 9.0; (c) pH 7.4; (d) pH 5.2). Little fluctuation of PL intensities was observed for all the samples. (e) Relative photoluminescence intensities (at 700 nm) of MPA-QDs stored in 1× PBS for 0, 1, 2, 3, 7, 10, 15, 20 days.

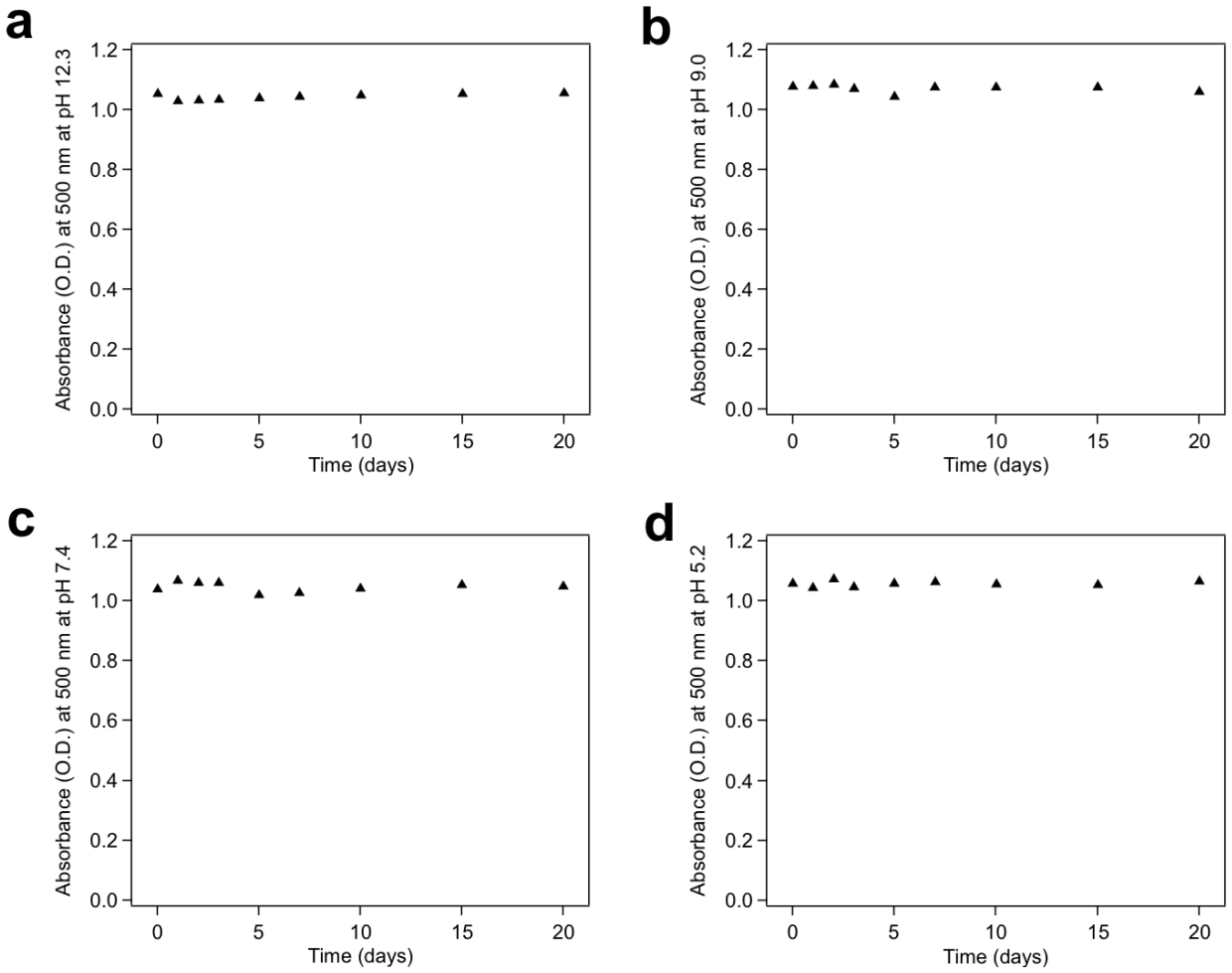

Figure S9. Absorbance (at 500 nm) of BSA-QDs stored at different pHs for 0, 1, 2, 3, 5, 7, 10, 15, and 20 days ((a) pH 12.3; (b) pH 9.0; (c) pH 7.4; (d) pH 5.2). Little fluctuation of QD absorbance was observed for all the samples.

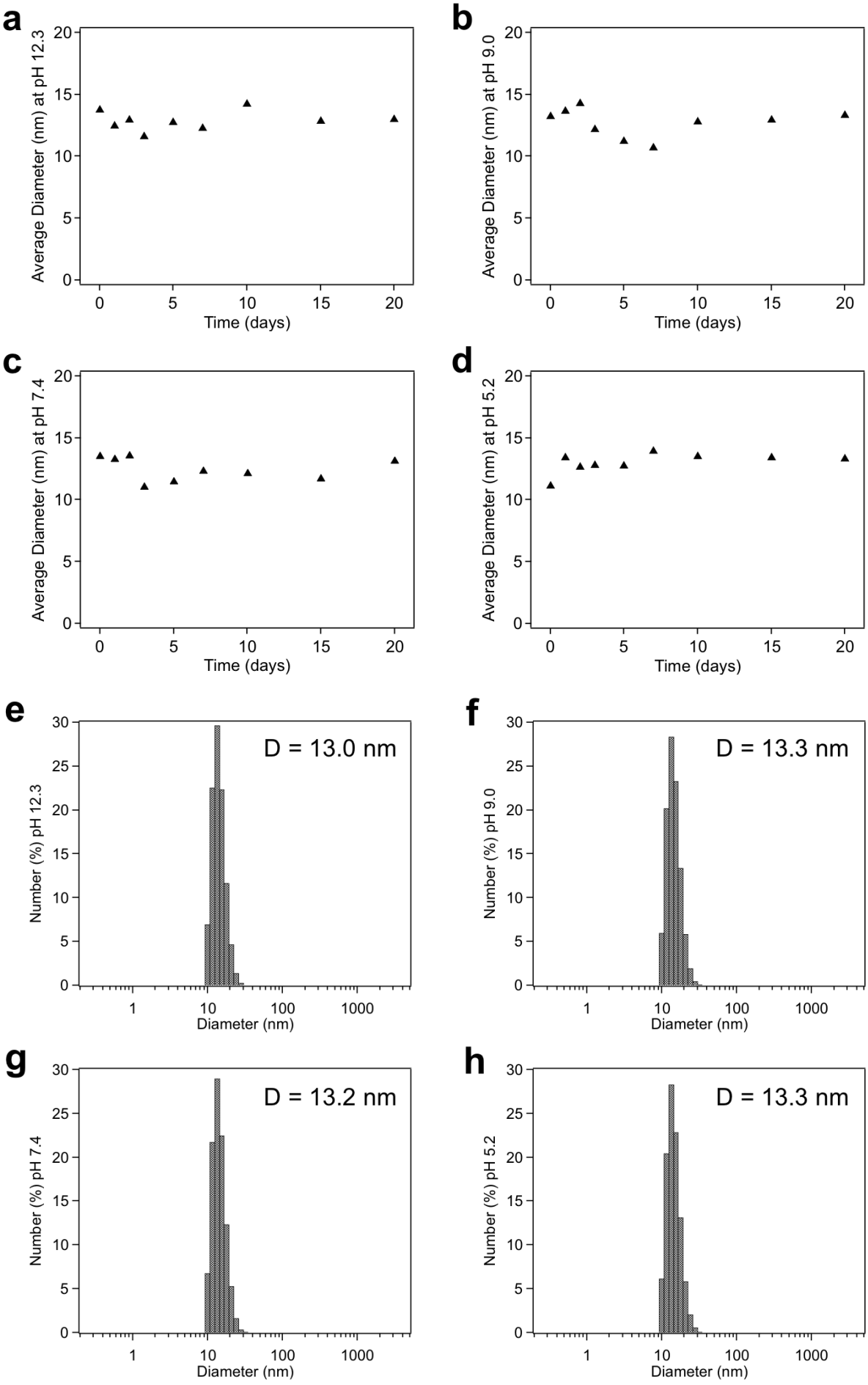
a
Average Diameter (nm) at pH 12.3
Time (days)
b
Average Diameter (nm) at pH 9.0
Time (days)
c
Average Diameter (nm) at pH 7.4
Time (days)
d
Average Diameter (nm) at pH 5.2
Time (days)
e
Number (%) pH 12.3
D = 13.0 nm
Diameter (nm)
f
Number (%) pH 9.0
D = 13.3 nm
Diameter (nm)
g
Number (%) pH 7.4
D = 13.2 nm
Diameter (nm)
h
Number (%) pH 5.2
D = 13.3 nm
Diameter (nm)

Figure S10. (a)-(d) DLS measurements of the average hydrodynamic diameters of BSA-QDs stored at different pHs for 0, 1, 2, 3, 5, 7, 10, 15, and 20 days ((a) pH 12.3; (b) pH 9.0; (c) pH 7.4; (d) pH 5.2). No aggregation was observed for all the samples. (e)-(h) DLS measurements of hydrodynamic diameters of BSA-QDs stored at different pHs for 20 days ((e) pH 12.3; (f) pH 9.0; (g) pH 7.4; (h) pH 5.2) The size distribution profiles of BSA-QDs stored for 20 days are quite similar to the freshly prepared BSA-QDs (Figure S7b).

3.2 Colloidal stability of FA-QDs

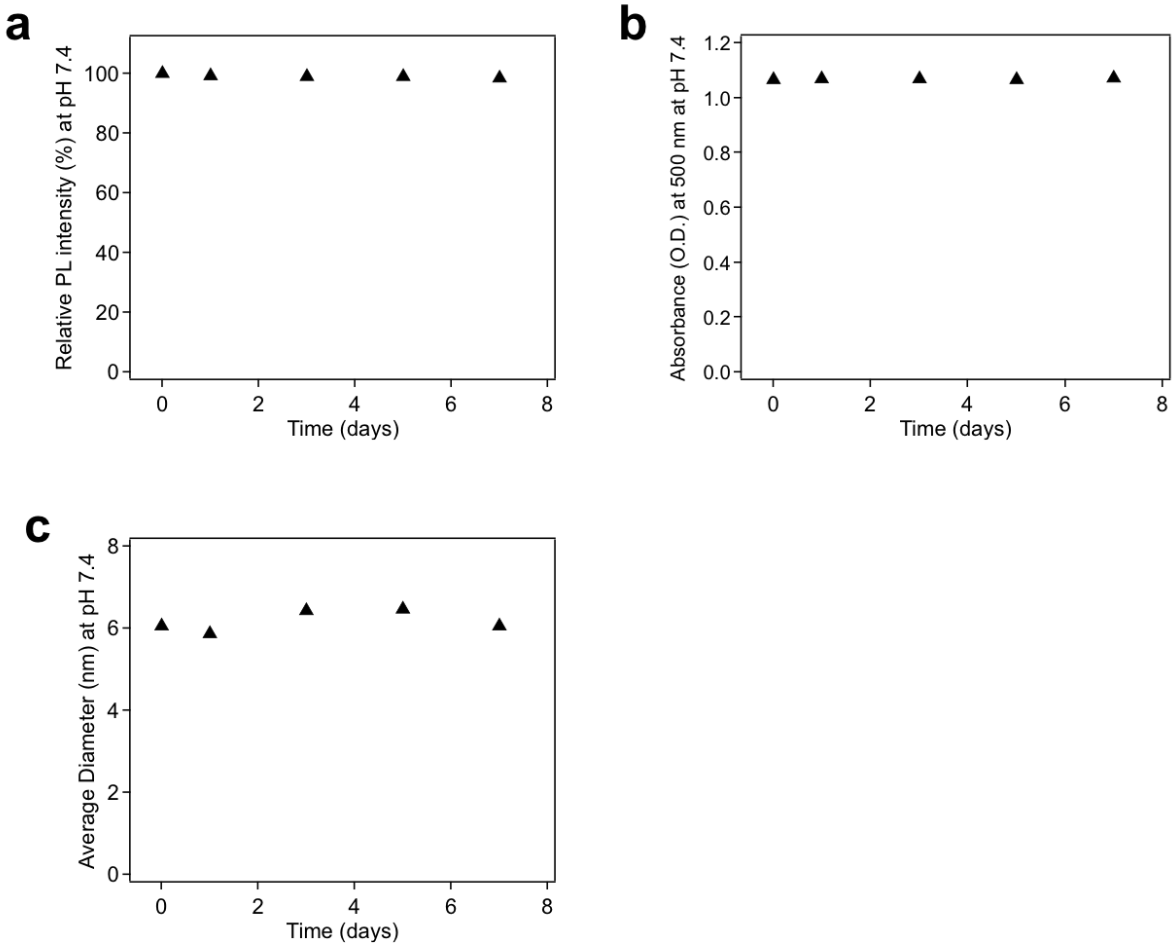

Figure S11. Colloidal stability measurements of FA-QDs. (a) Relative photoluminescence intensity of FA-QDs stored at pH 7.4 for 0, 1, 3, 5, 7 days. (b) Absorbance (at 500 nm) of FA-QDs stored at pH 7.4 for 0, 1, 3, 5, 7 days. (c) Average hydrodynamic diameters of FA-QDs stored at pH 7.4 for 0, 1, 3, 5, 7 days. FA concentration for QDs synthesis is 10 mM.

3.3 Photostability of BSA-QDs, MPA-QDs, and CdSe QDs

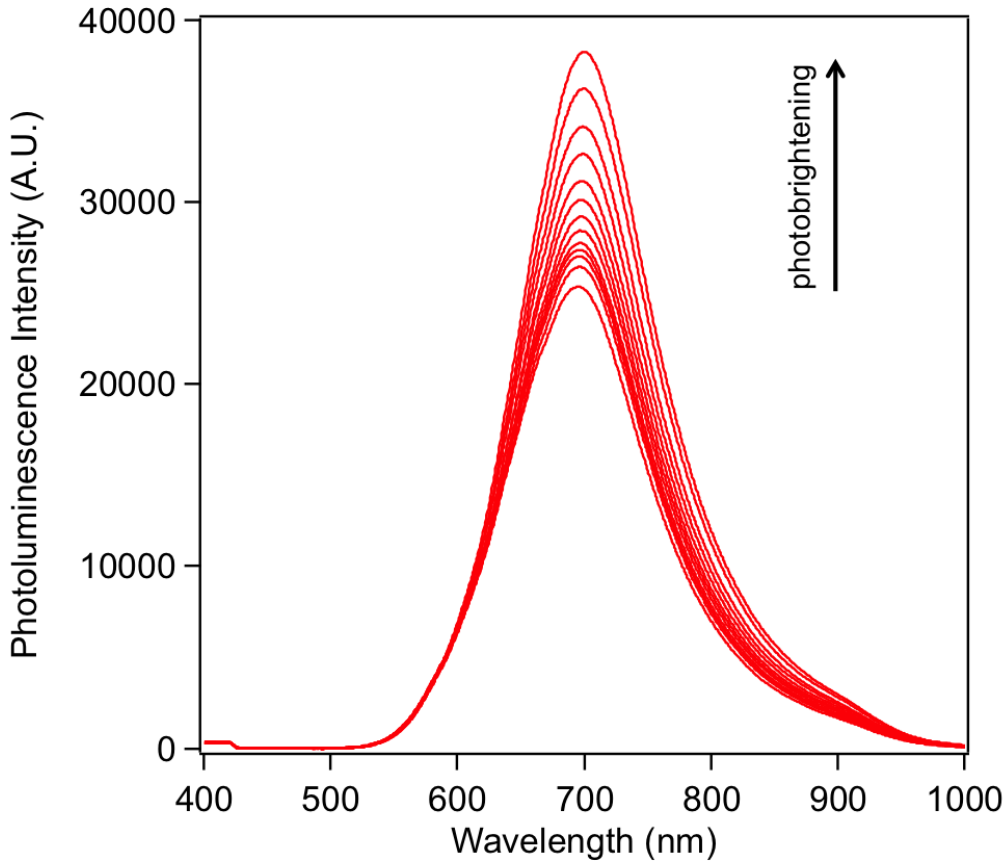

Figure S12. Photostability measurements of BSA-functionalized $Zn_xHg_{1-x}Se$ QDs. The QDs were continuously excited with a 405 nm laser (110 mW) and the photoluminescence spectra were recorded at different time points (0, 0.5, 1, 3, 5, 8, 12, 15, 20, 30, 40, 50, 60 min).

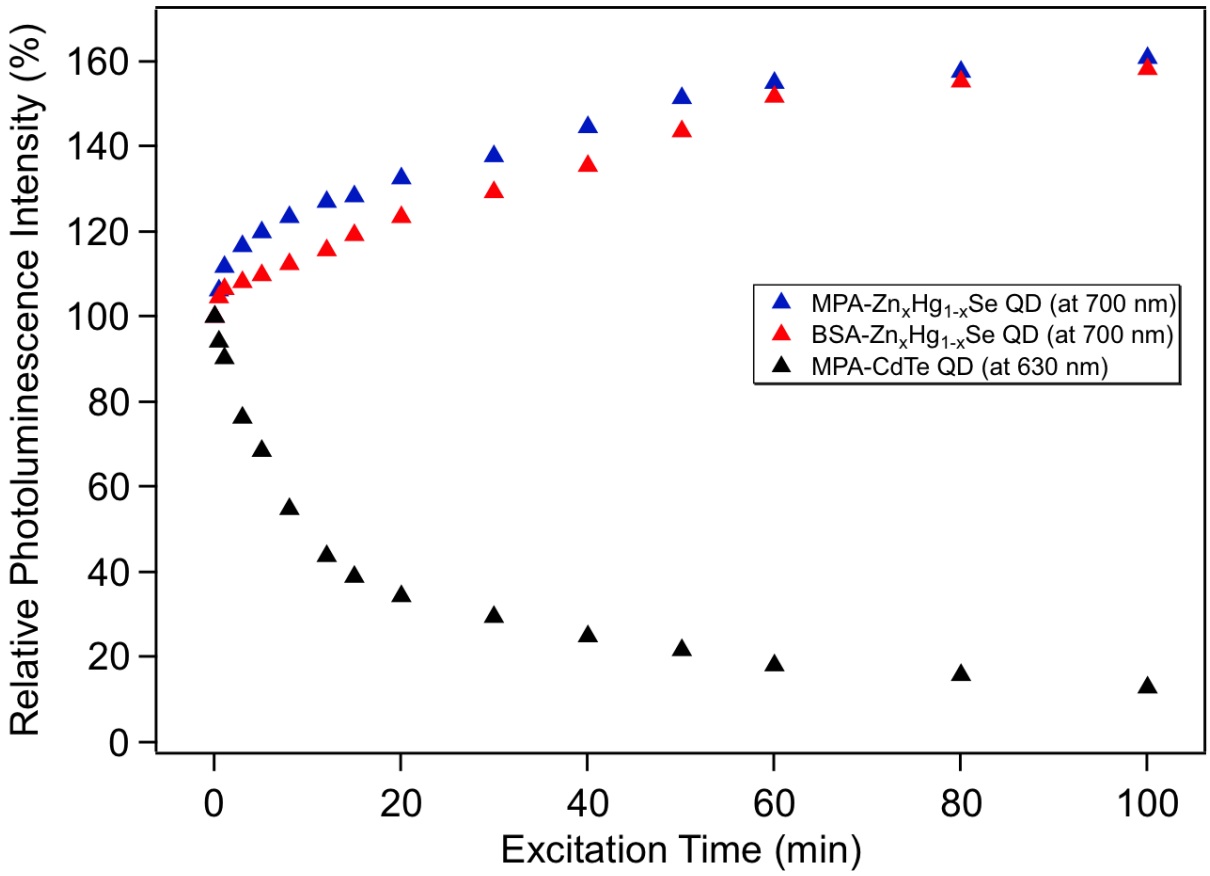

Figure S13. Comparison of photostabilities of MPA-$Zn_xHg_{1-x}Se$ QDs, BSA-$Zn_xHg_{1-x}Se$ QDs, and MPA-CdTe QDs under continuous excitation with a 405 nm laser (110 mW) for 100 minutes.

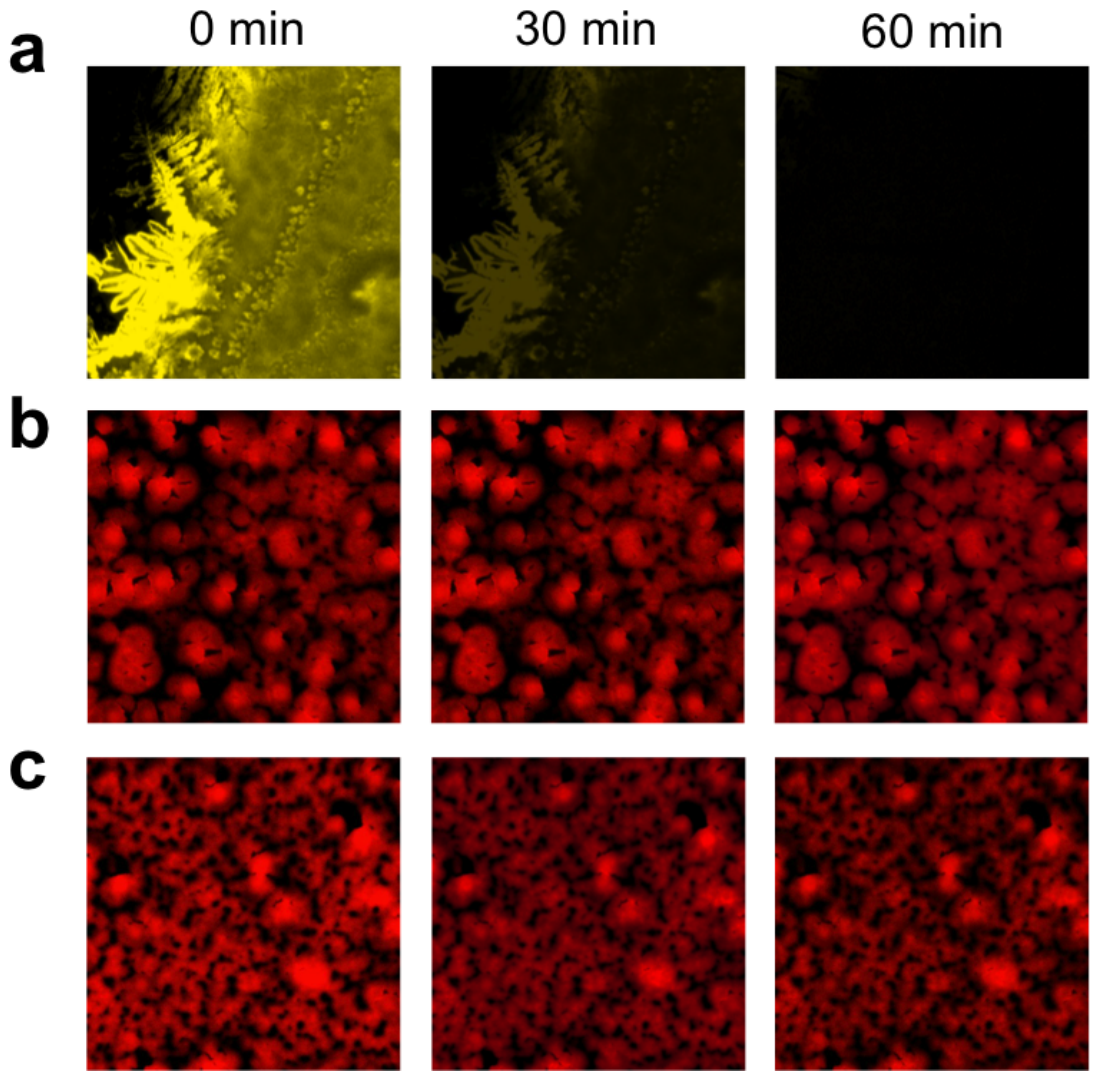

Figure S14. Comparison of photostabilities of (a) MPA-CdSe QDs, (b) MPA-$Zn_xHg_{1-x}Se$ QDs, and (c) BSA-$Zn_xHg_{1-x}Se$ QDs under continuous excitation with a 365 nm UV lamp (8 W) for 30 and 60 minutes. A drop of QD solution was added into each well of a 8-well chamber and then air-dried to form a QD film for photostability study. The fluorescence image of each QD film was recorded on an Olympus IX71 epifluorescence microscope and the acquisition time was 1 ms for all the images. The CdSe QDs film was quickly photobleached after 30 min excitation whereas the photoluminescence of MPA-$Zn_xHg_{1-x}Se$ QDs and BSA-$Zn_xHg_{1-x}Se$ QDs was retained after 60 min excitation, indicating the photostability of $Zn_xHg_{1-x}Se$ QDs is much higher than CdSe QDs. The CdSe QDs were synthesized directly in NH_4HCO_3 (pH 9.0) solution using $CdCl_2$ and NaHSe as precursors and MPA as stabilizing agents.

3.4 Choice of pH for the synthesis of biofunctionalized QDs

In our study all the biofunctionalized QDs were synthesized at pH 12.3. The choice of pH for QD synthesis is dependent on the pIs of proteins. More specifically, if the protein has a low pI value (e.g. BSA pI=5.3) the QDs can also be synthesized at neutral pHs (e.g. 7.4). If the protein has a high pI value (e.g. lysozyme pI=11.4) the synthesis needs to be conducted at high pHs (12.3) to avoid QD aggregation during synthesis. Importantly, all the as-prepared protein-functionalized QDs remain stable when the pH changes from 12.3 to 7.4 after QD synthesis. Also, it is noteworthy that when the pH changes back to 7.4 the QD-associated proteins (BSA and lysozyme) maintain their native structure and activity. Therefore, the high pH used for QDs synthesis would not affect the applicability of these QDs. In addition, since FA molecules are highly soluble at basic conditions and the peptide (HHHHHHCGKRK) has a high pI value (10.6), the FA and peptide-functionalized QDs were also synthesized at pH 12.3. The FA-QDs and peptide-QDs also remain stable when the pH is adjusted back to 7.4 after synthesis. To unify the synthetic protocol we choose pH 12.3 for all the QD synthesis.

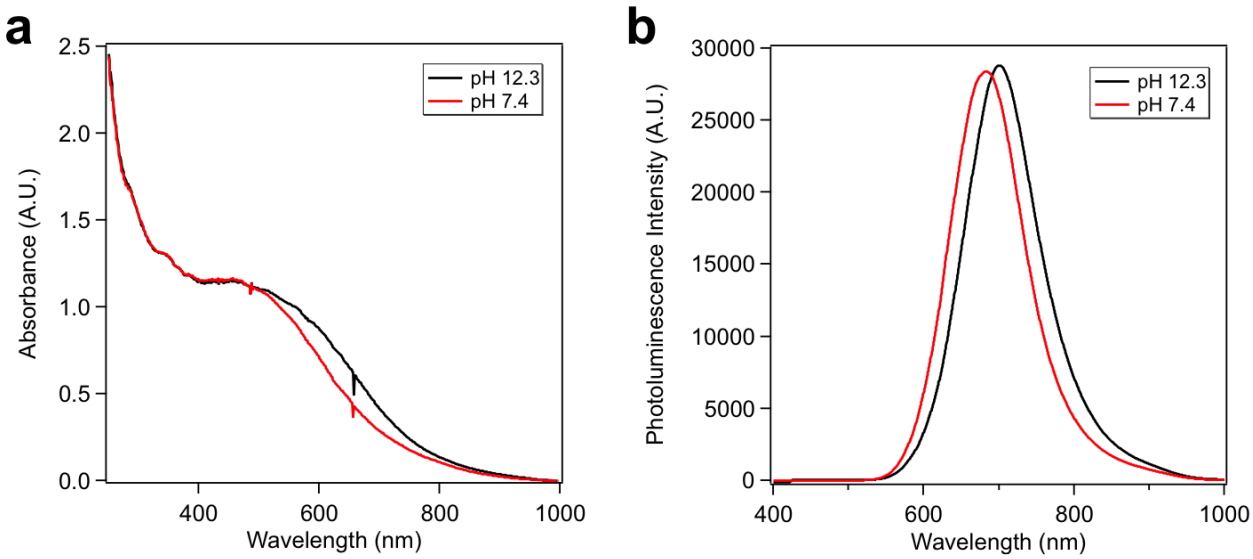

Figure S15. Absorption spectra (a) and photoluminescence spectra (b) of BSA-functionalized $Zn_xHg_{1-x}Se$ QDs synthesized at pH 12.3 and pH 7.4.

4. Analysis of biofunctionalization of QDs

4.1 Circular dichroism study on BSA-QDs

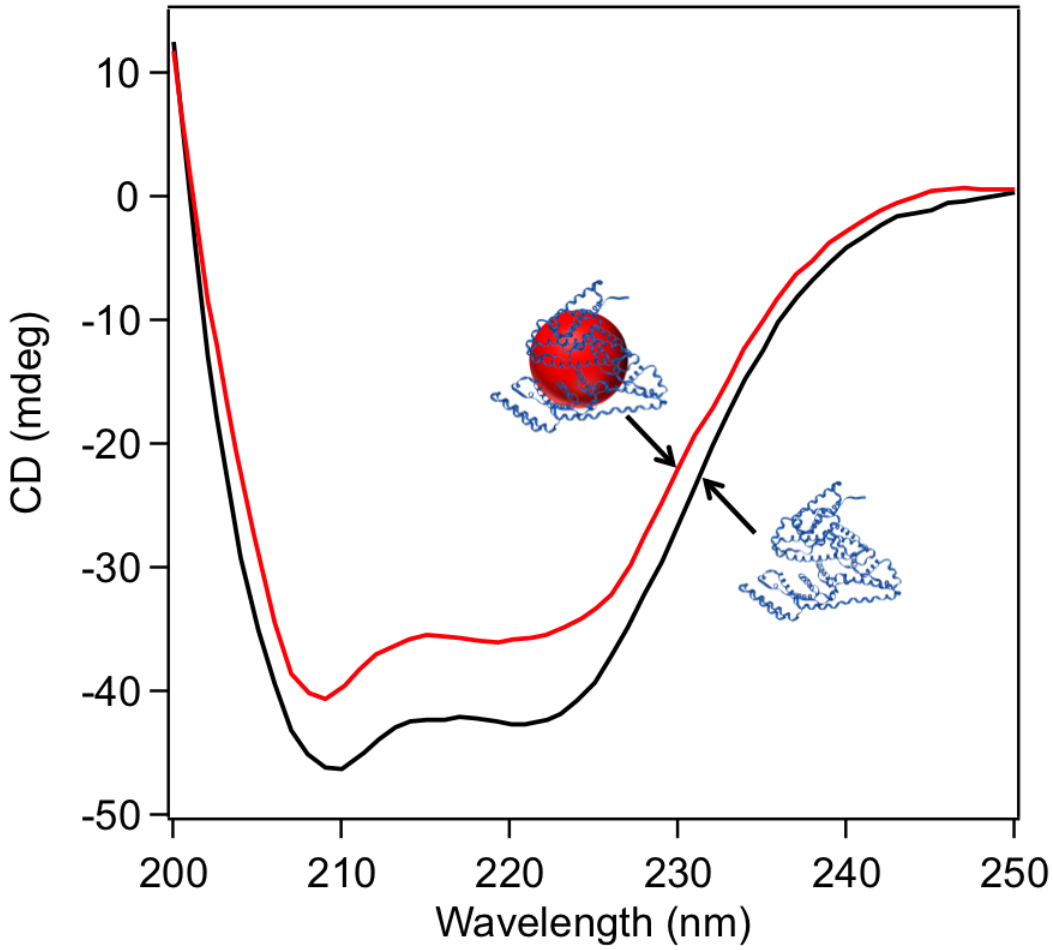

Figure S16. Circular dichroism spectra of native BSA and QD-associated BSA. The bands at 222 nm and 208 nm are due to α-helix in BSA.

4.2 Gel electrophoresis of protein- and peptide-functionalized QDs

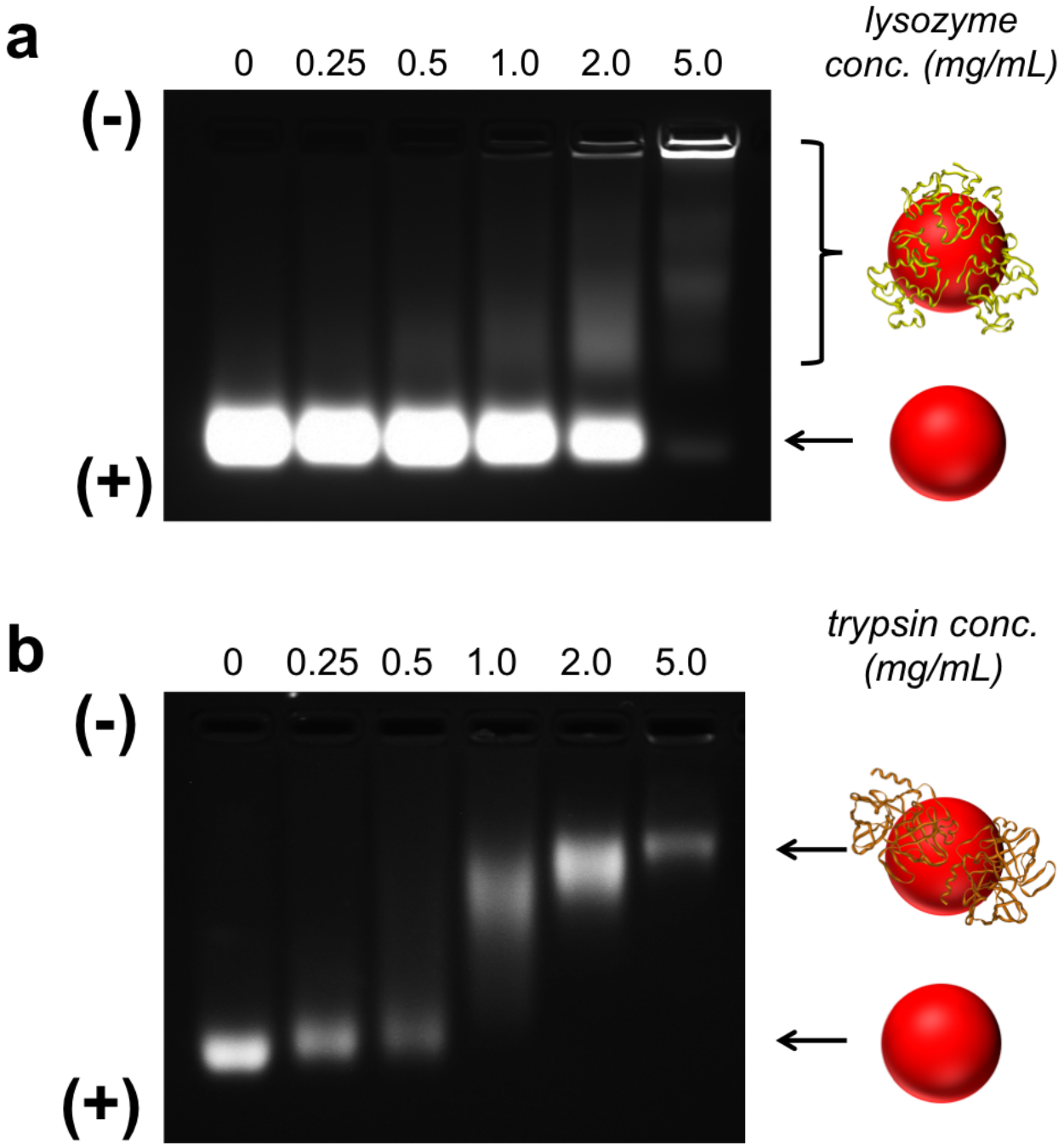

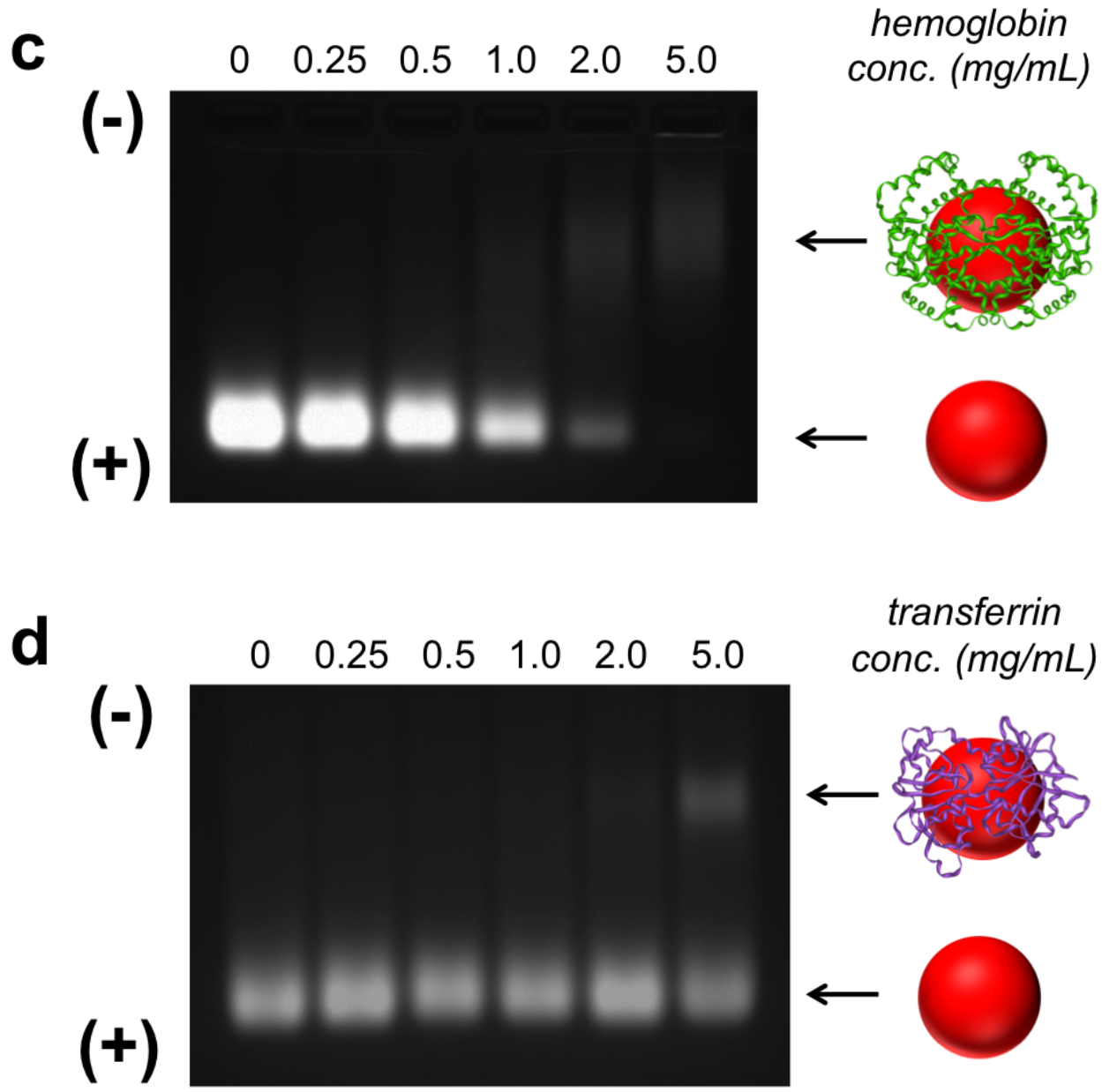

Figure S17. Agarose gel electrophoresis of MPA-QDs and protein-QDs synthesized at various protein concentrations (0, 0.25, 0.5, 1.0, 2.0, and 5.0 mg/mL). (a) lysozyme QDs; (b) trypsin-QDs; (c) hemoglobin-QDs (the band of hemoglobin-QDs is weak because of PL quenching by hemoglobin); (d) transferrin-QDs.

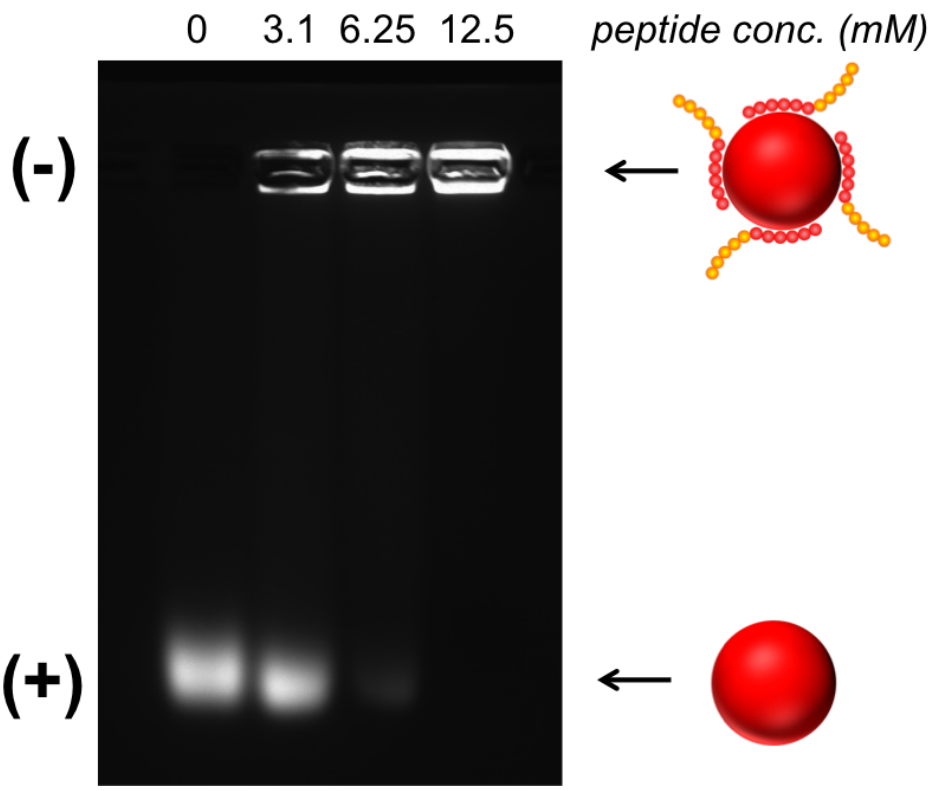

Figure S18. Agarose gel electrophoresis of MPA-QDs and peptide-QDs synthesized at various peptide concentrations (0, 3.1, 6.25, 12.5 mM). The retarded mobility of peptide-functionalized QDs is mainly due to the neutralization of negative charge on QD surface by positively charged peptides.

4.3 Isolation of pure protein-QD conjugates from agarose gel

We first conducted an agarose gel electrophoresis for the crude BSA-QDs sample (2 mg/mL BSA) which exhibits two fluorescent bands corresponding to the BSA-QDs and MPA-QDs respectively. We then cut and collect the agarose gel slice containing each type of QDs and then extract the pure conjugates by compressing and liquifying the gel. After that we concentrated each type of the extracted QDs and performed another agarose gel electrophoresis to check the purity and integrality of each pure QD sample (Figure S16). Our results show that the pure protein-QD conjugates can be fully recovered from agarose gel.

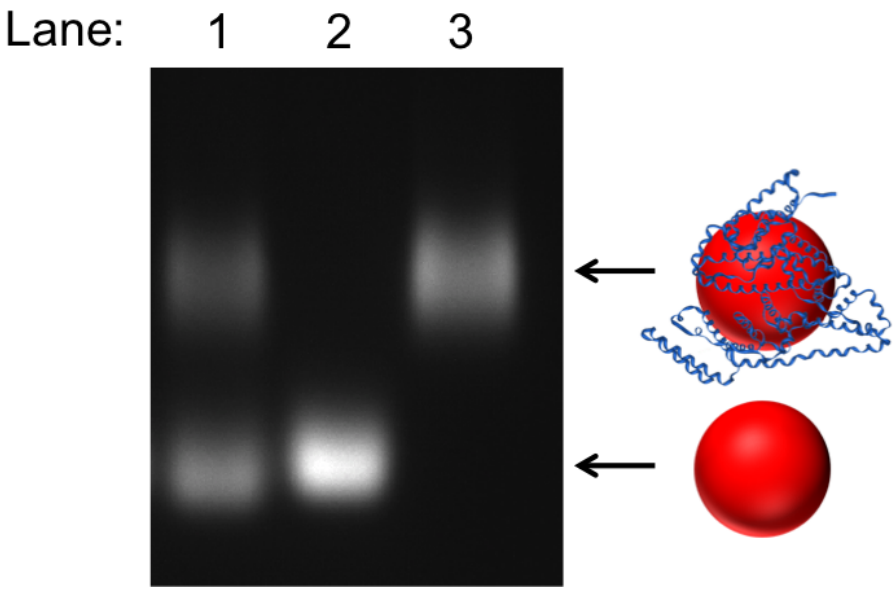

Figure S19. Agarose gel electrophoresis of crude BSA-QDs sample (2 mg/mL BSA) (lane 1), QDs isolated from the lower band of the crude sample (lane 2), QDs isolated from the upper band of the crude sample (lane 3).

4.4 Absorption spectrum of native hemoglobin

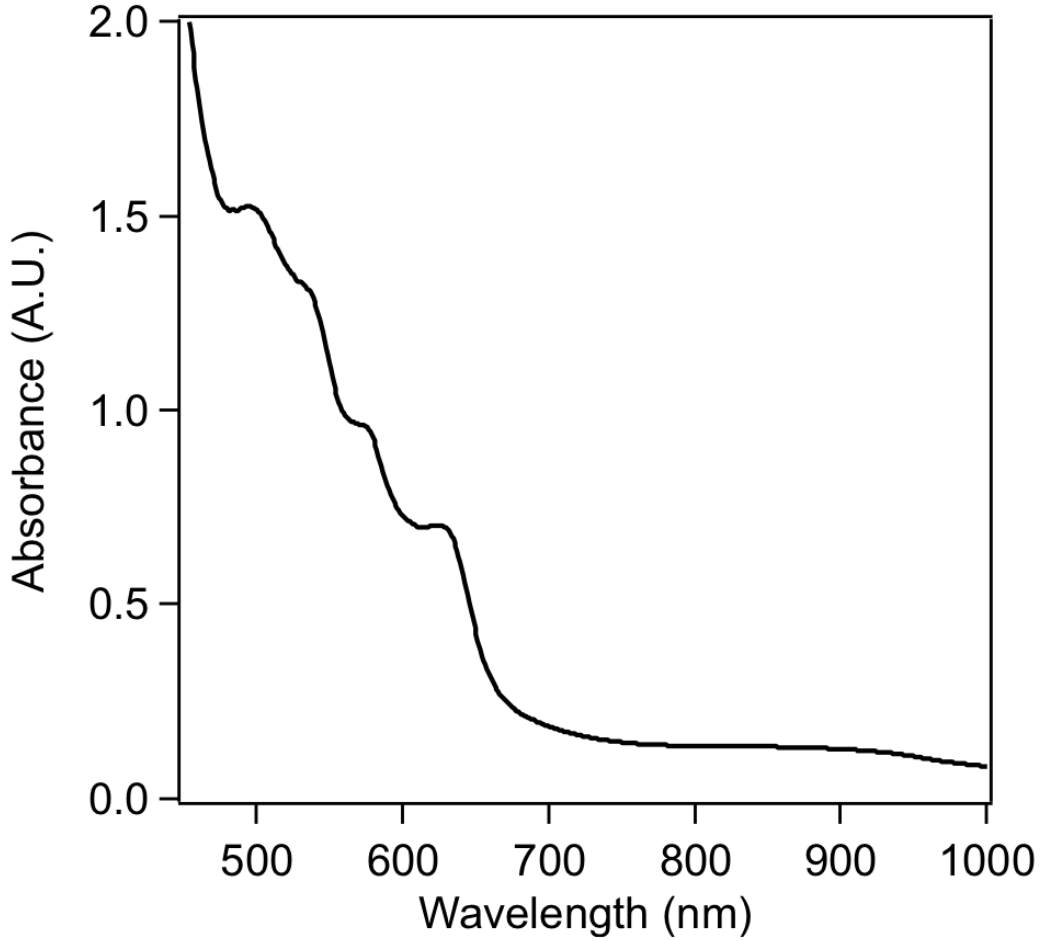

Figure S20. Absorption spectrum of native hemoglobin.

4.5 Fluorescence microscopy images of HeLa cells treated with transferrin-QDs acquired with 10× and 40× objectives

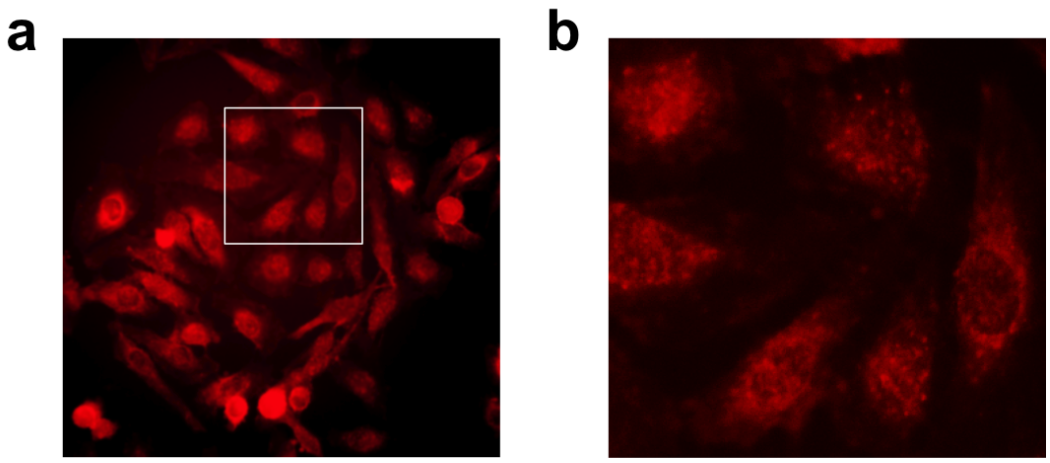

Figure S21. Fluorescence microscopy images of HeLa cells treated with transferrin-QDs acquired with a 10× objective (a) and a 40× objective (b). The white box in (a) indicates the field of view in (b). Punctate patterns of cell staining could be clearly visualized in (b).

4.6 FTIR measurements of FA-QDs

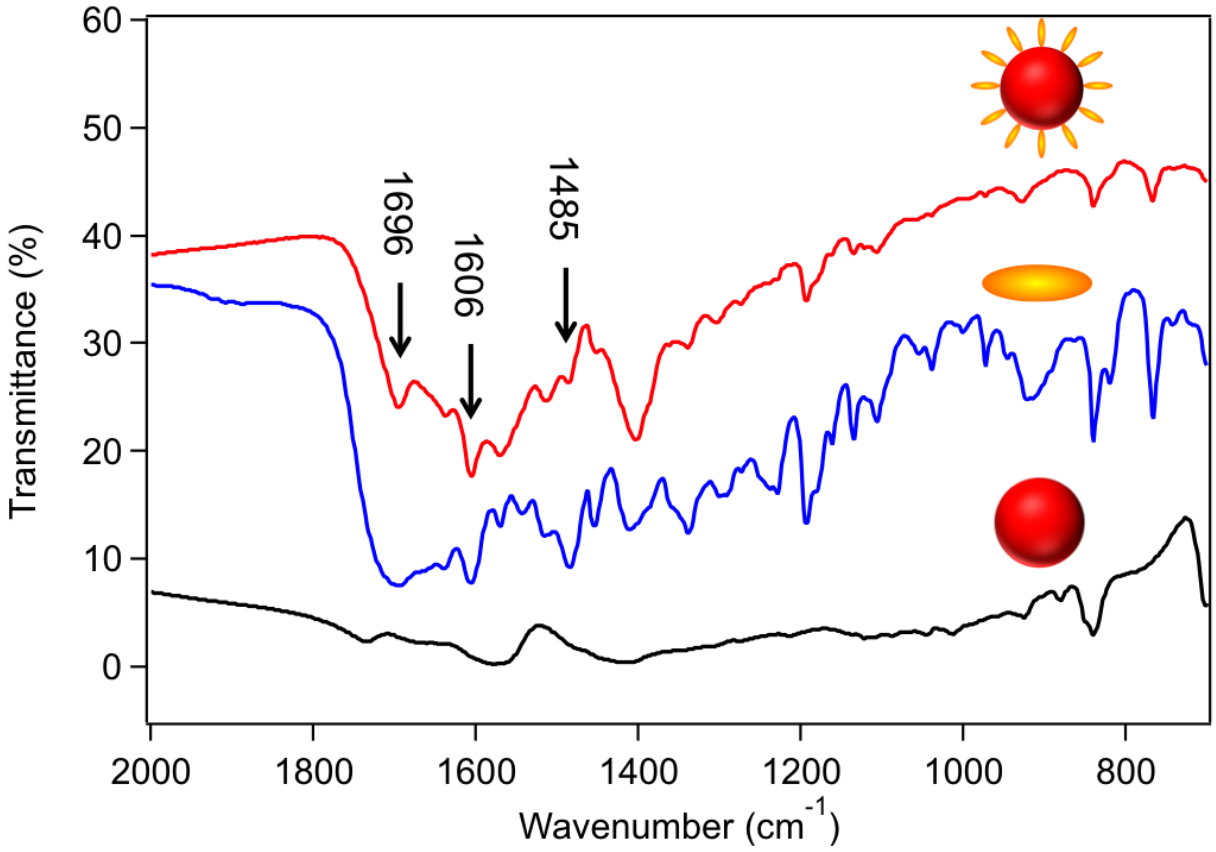

Figure S22. FTIR spectra of folic acid-QDs (red), free folic acid (blue), and MPA-QDs (black). The spectra of folic acid-QDs and free folic acid both exhibit characteristic IR absorption peaks of folic acid at 1606 cm^{-1} (-NH group), 1696 cm^{-1} (C=O bond), and 1485 cm^{-1} (phenyl ring), confirming the attachment of folic acid on QDs.

4.7 Photoluminescence quenching of FA-QDs

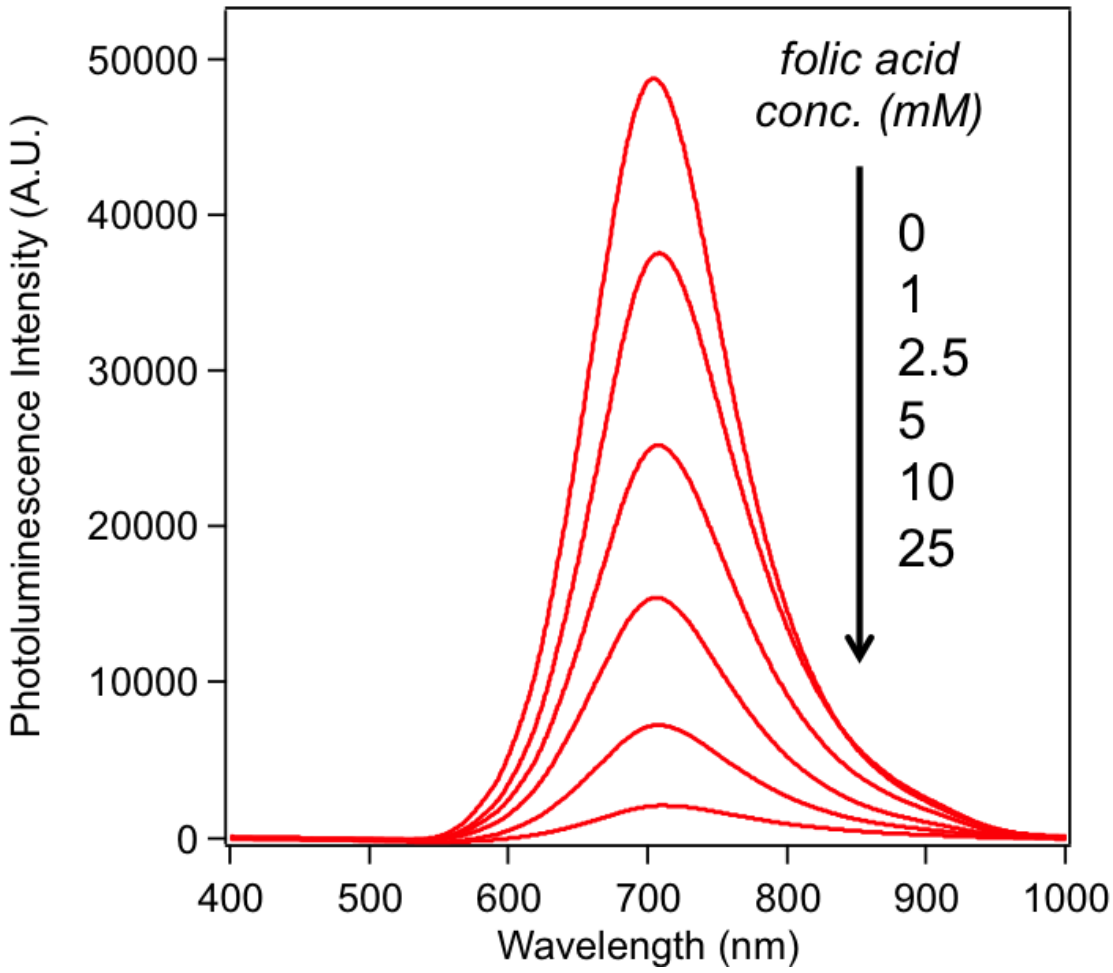

Figure S23. Photoluminescence spectra of $Zn_xHg_{1-x}Se$ QDs synthesized at different folic acid concentrations (0, 1, 2.5, 5, 10, and 25 mM). As the folic acid concentration increases, the QD photoluminescence is more efficiently quenched.

5. Analysis of linking chemistry for protein attachment to QDs

5.1 Chemical modification of five types of amino acid residues in BSA molecules

There are a variety of amino acid residues including Asp/Glu (carboxyl group), His (imidazole), Tyr (hydroxyl group), Lys (amino group), and Cys (thiol group) that could interact with Zn^{2+} ions and participate in the QD attachment (Trzaskowski, B.; Adamowicz, L.; & Deymier, P. *J. Biol. Inorg. Chem.* **2008**, *13*, 133-137). Since there are a number of such residues present in a protein molecule, it is expectable that the protein attachment results from the cooperative binding of different residues with the QD. To further deconvolute the role of each type of amino acid residue in QD attachment, we performed selective chemical modification of each type of amino acid residue (amino group, thiol group, carboxyl group, imidazole group, hydroxyl group) in BSA respectively in order to block its interaction with the QD (**Figure S21**). Then we used each chemically modified BSA to synthesize QDs and quantitate the protein functionalization efficiency for the QDs to find out the contribution of each type of amino acid residue to protein attachment.

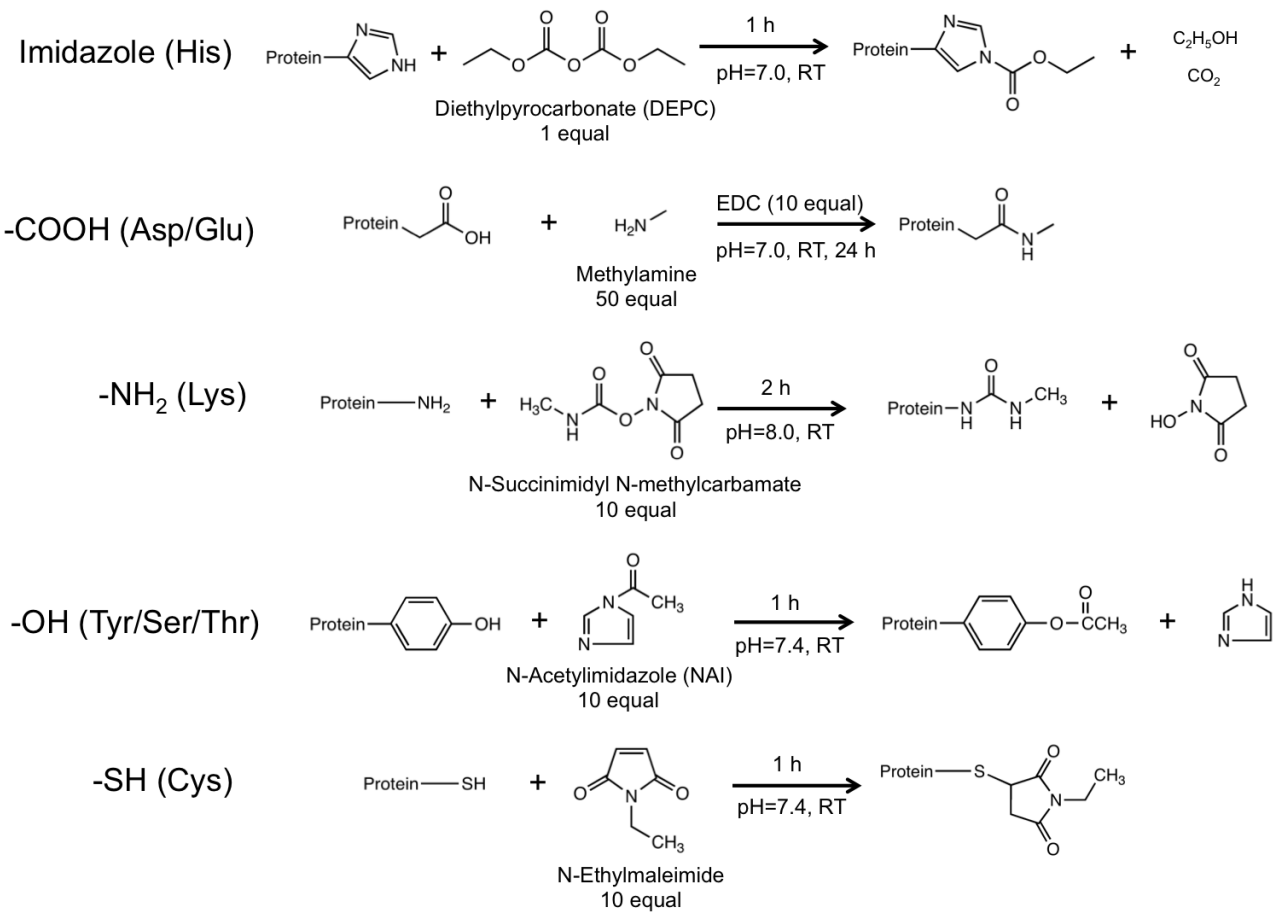

Figure S24. Chemical reactions for chemical modification of five types of amino acid residues (imidazole, -COOH, $-NH_2$, -OH, and –SH).

Experimental section for chemical modification of amino acid residues

Materials

1-Acetylimidazole (NAI, 98.0 %), N-succinimidyl N-methylcarbamate (NHS, 97.0 %), and diethylpyrocarbonate (DEPC, 99.0 %) were purchased from Sigma-Aldrich. N-Ethylmaleimide (99.0 %), methylamine (40% w/w aq. soln), and 1-(3-dimethylaminopropyl)-3-ethylcarbodiimide hydrochloride (EDC, 98.0 %) were purchased from Alfa Aesar.

Protocol

BSA powder was dissolved in 1× PBS to the concentration of 100 mg /mL; 1-acetylimidazole (NAI) was dissolved in 1/2 v/v DMSO/H_2O solution to the concentration of 1.333 M; N-succinimidyl N-methylcarbamate (NHS) was dissolved in DMSO to the concentration of 0.5 M; diethylpyrocarbonate (DEPC) was diluted in anhydrous ethanol to the concentration of 1 M; N-ethylmaleimide was dissolved in 1/100 v/v DMSO/H_2O solution to the concentration of 100 mM; 1-(3-dimethylaminopropyl)-3-ethylcarbodiimide hydrochloride (EDC) was dissolved in water to the concentration of 1 M; methylamine (40% w/w aq. Soln) of 12.88 M was directly used. All the materials above were freshely prepared for BSA modification. The total reaction volume of each chemical modification reaction is 500 uL. The BSA concentration in each reaction is 5 mg/ mL.

10 equivalents of NAI were used to modify the hydroxyl groups (-OH) of tyrosine, serine, and threonine and the reaction was performed in 1× PBS (pH=7.4) for 1 hour at room temperature. 10 equivalents of NHS were used to modify the amino groups (-NH_2) of lysine and the N terminus and the reaction was performed in 1× PBS (pH=8.0) for 2 hours at room temperature. 10 equivalents of N-ethylmaleimide were used to modify the thiol groups (-SH) of cysteine and the reaction was performed in 1× PBS (pH=7.4) for 1 hour at room temperature. 1 equivalent of DEPC was used to modify the imidazole groups of histidine and the reaction was performed in 1× PBS (pH=7.0) for 1 hour at room temperature. 10 equivalents of EDC and 50 equivalents of methylamine were used to modify the carboxylic groups (-COOH) of glutamic acid, aspartic acid, and the C terminus and the reaction was performed in 1× PBS (pH=7.0) for 24 hours at room temperature. After each reaction the modified BSA product was purified twice with a Microsep^{TM} Advance Centrifugal Device (YM-3, Pall Corporation) via centrifugation at 13500 rpm for 8 min. The purified product was then recovered to the desired volume in 1× PBS (pH=7.4) for QDs synthesis. The protocol for QDs synthesis with chemically modified BSA is the same as unmodified BSA.

5.2 Determination of functionalization efficiencies of BSA-QDs synthesized with unmodified and modified BSA

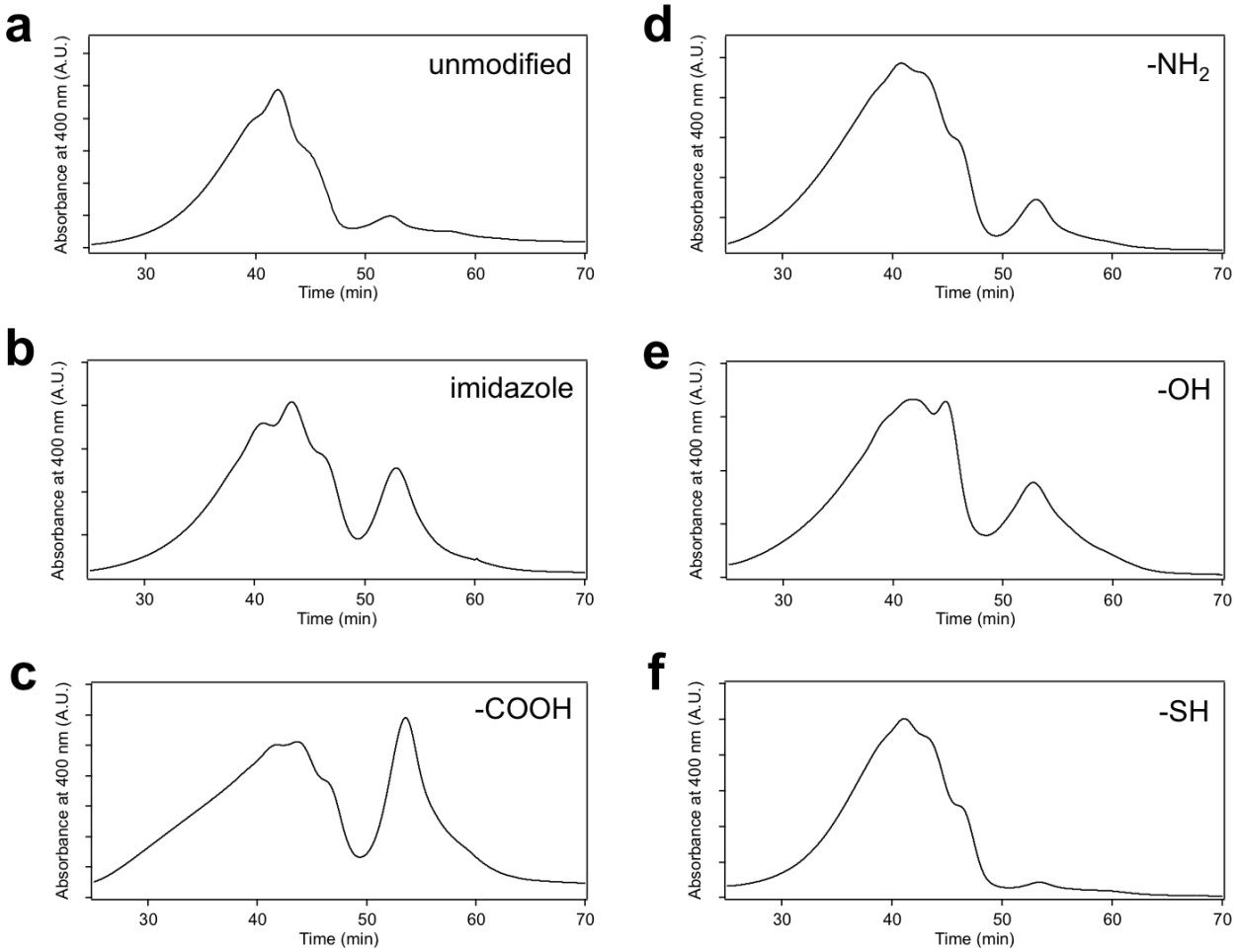

Figure S25. Gel filtration chromatography of BSA-QDs synthesized with unmodified and chemically modified BSA. (a) unmodified BSA; (b) BSA with modified imidazole (His); (c) BSA with modified –COOH (Asp/Glu/C-terminus); (d) BSA with modified $–NH_2$ (Lys/N-terminus); (e) BSA with modified –OH (Tyr/Ser/Thr); (f) BSA with modified –SH (Cys).

Modification types	QDs functionalization efficiency
Unmodified	95%
Imidazole (His)	74%
-COOH (Asp/Glu/C-terminus)	65%
$-NH_2$ (Lys/N-terminus)	85%
-OH (Tyr/Ser/Thr)	75%
-SH (Cys)	95%

Table S1. Functionalization efficiencies of BSA-QDs synthesized with unmodified and chemically modified BSA. The functionalization efficiency is calculated according to the gel filtration chromatography results in **Figure S22**. The carboxyl group, imidazole group, and hydroxyl group play an important role in protein attachment. Cysteine residues have almost no effect on protein attachment since most of cysteine residues form disulfide bonds in proteins.

5.3 Occurrences of critical amino acid residues in BSA sequence and in a large population of protein sequences

BSA sequence (583 aa)

```
1   dthkseiahr fkdlgeehfk glvliafsqy lqqcpfdehv klvneltefa ktcvadesha
61  gcekslhtlf gdelckvasl retygdmadc cekqeperne cflshkddsp dlpklkpdpn
121 tlcdefkade kkfwgkylye iarrhpyfya pellyyanky ngvfqeccqa edkgacllpk
181 ietmrekvlt ssarqrlrca siqkfgeral kawsvarlsq kfpkaefvev tklvtdltkv
241 hkecchgdll ecaddradla kyicdnqdti ssklkeccdk pllekshcia evekdaipen
301 lppltadfae dkdvcknyqe akdaflgsfl yeysrrhpey avsvllrlak eyeatleecc
361 akddphacys tvfdklkhlv depqnlikqn cdqfeklgey gfqnalivry trkvpqvstp
421 tlvevsrslg kvgtrcctkp esermpcted ylslilnrlc vlhektpvse kvtkcctesl
481 vnrrpcfsal tpdetyvpka fdeklftfha dictlpdtek qikkqtalve llkhkpkate
541 eqlktvmenf vafvdkccaa ddkeacfave gpklvvstqt ala
```

Amino acids (aa)	His (imidazole)	Asp/Glu (-COOH)	Tyr (-OH)	Lys ($-NH_2$)	Cys (-SH)
Occurrence in BSA (%) (number of aa)	**2.9% (17)**	**17.0% (99)**	**3.4% (20)**	10.1% (59)	6.0% (35)
Occurrence in a large protein population (%)	**2.2%**	**11.5%**	**3.3%**	5.8%	1.8%

Table S2. Occurrences of critical amino acid residues in BSA sequence and a large population of protein sequences (105990 sequences in the nonredundant OWL protein database (release 26.0 e) (G. Trinquier and Y.-H. Sanejouand *Protein Engineering* **1998,** *11*, 153-169))

The occurrences of Asp/Glu (-COOH), His (imidazole), and Tyr (-OH) within BSA and the large protein population are at similar levels. Therefore, it is expectable that this QD synthetic strategy would work for many other proteins.

5.4 Percentages of buried and exposed residues of critical amino acids in globular proteins

As reported by previous studies, most polar residues are on protein surface and most non-polar residues are inside globular proteins (J. Janin *Nature* **1979**, *277*, 491-492). The four types of critical amino acid residues for QD binding are all polar residues (imidazole (His), -COOH (Asp/Glu), -NH_2 (Lys), -OH (Tyr)) and therefore would be found mostly on protein surface. Below is a summary of the percentages of buried and exposed residues for these four types of amino acids in different proteins (Table S3). The data is adapted from a paper by C. H. Schein (*Nature Biotechnol*. **1990,** *8,* 308-317).

Amino acid residues	Percent buried residues	Percent exposed residues
Asp	10%	90%
Glu	20%	80%
His	19%	81%
Tyr	13%	87%
Lys	4.2%	95.8%

Table S3. Summary of percentages of buried and exposed residues of critical amino acids in globular proteins.

As shown in the above table, only small percentages of these residues are buried inside proteins and most of these residues are exposed and would be accessible for QD binding.

6. Mechanism study of protein-mediated QDs formation

6.1 Probing the interaction of protein with metal ions and QDs using FTIR

Previous studies on QD formation mechanisms (e.g. S. Hinds *et al. J. Am. Chem. Soc*. **2006,** *128*, 64-65; B. A. Kairdolf *et al*. *J. Am. Chem. Soc.* **2008,** *130*, 12866-12867.) suggest that the colloidal QD formation goes through four stages including: i) the chelation of metal ions with ligands; ii) the formation of nuclei after introducing anion precursors; iii) the subsequent growth of nuclei to form nanocrystals; and iv) passivation of QD surface with ligand molecules. In the paper by S. Hinds *et al*. (*J. Am. Chem. Soc*. **2006,** *128*, 64-65) the authors conducted FTIR experiments to explore the binding of ligand molecules (nucleotides) with metal ions which is a primary step for controlled QD seeding (nucleation) and growth. In this study we first conducted FTIR experiments to probe the interactions of BSA with metal ions and QDs during the course of QD formation.

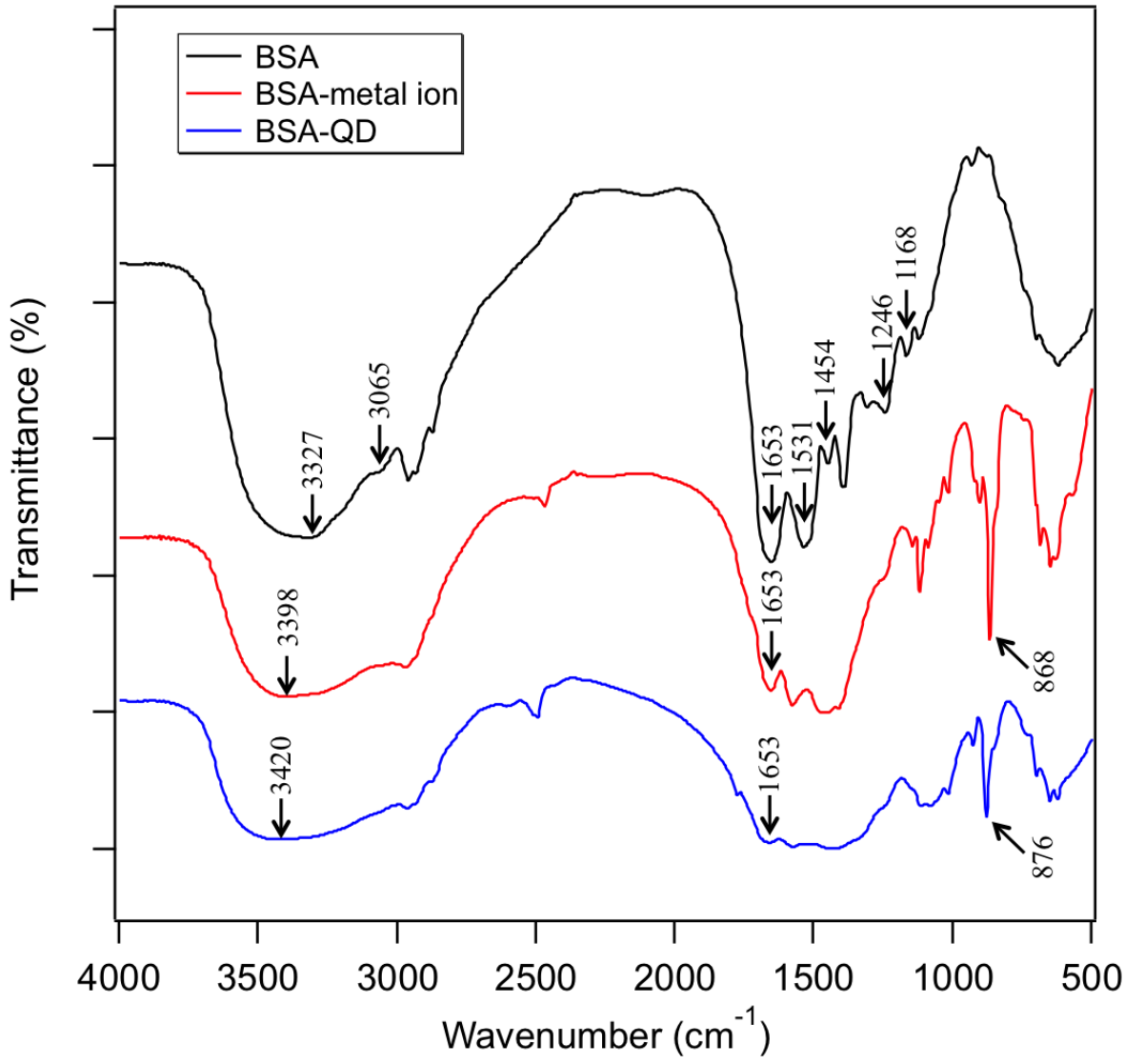

Figure S26. FTIR spectra of free BSA, BSA-metal ion complex, and BSA-QD complex.

FTIR spectra of free BSA, BSA-metal ion, and BSA-QD were recorded to probe the interactions of BSA with metal ions and QDs during the course of QD synthesis. As shown in Figure S24, the broad peak of free BSA at 3327 cm^{-1} is attributed to the O-H stretch of the phenol group. This peak shifts to higher wavenumber for BSA-metal ion (3398 cm^{-1}) and BSA-QD (3420 cm^{-1}), revealing the interaction of the phenol group of tyrosine residue with metal ions and QDs. The peak of free BSA at 3065 cm^{-1} is attributed to the N-H stretch of the primary amine. This peak disappears in BSA-metal ion and BSA-QD complex, suggesting that the amino groups of lysine residues bind with the metal ions and QDs. The peak at 1653 cm^{-1} is due to the C=O stretch of the carboxyl group. The intensity of this peak is significantly attenuated for BSA-metal ion and BSA-QD complex, indicating the interaction of carboxyl group with metal ions and QDs. The peak of free BSA at 1531 cm^{-1} is due to the N-H bend of the amino group. This peak disappears in BSA-metal ion and BSA-QD complex, indicating the interaction of the amino groups with metal ions and QDs. The peak of free BSA at 1454 cm^{-1} is due to the C-N stretch of the imidazole group. This peak is significantly attenuated in BSA-metal ion and BSA-QD complex, indicating the interaction of histidine residue with metal ions and QDs. The peak of free BSA at 1246 cm^{-1} is due to the C-O stretch of the phenol group of tyrosine residue. This peak is significantly attenuated in BSA-metal ion and BSA-QD complex, suggesting that the tyrosine residue binds to metal ions and QDs. The peak at 1168 cm^{-1} is due to the C-O stretch of the carboxyl group of Asp and Glu. This peak disappears in BSA-metal ion and BSA-QD complex, indicating the interaction of carboxyl group with metal ions and QDs. The appearance of new peaks at 868 cm^{-1} (BSA-metal ion) and 876 cm^{-1} (BSA-QD) also indicates the interactions of BSA with metal ions and QDs. Overall, these results suggest that the BSA molecules chelate with the metal ions at the initial stage and remain bound to the QDs after QD formation. (The peak assignment is based on the data in a review article (A. Barth *BBA-Bioenergetics* **2007,** *1767*, 1073-1101.))

6.2 Monitoring the nucleation and QD growth via UV-Vis spectroscopy and TEM

We investigated nuclei formation and QD growth using UV-Vis spectroscopy and TEM. In the paper by B. A. Kairdolf *et al* (*J. Am. Chem. Soc.* **2008,** *130*, 12866-12867) the authors demonstrated that the growth of QDs from small nuclei is accompanied by a gradual red shift of their absorption spectra due to the increased nanocrystal sizes. In our case because the Se precursors are highly reactive with Zn^{2+} ions in aqueous solution at ambient conditions and hence the QD growth proceeds extremely fast (<1 second), it is impractical to resolve the nucleation and growth steps in such a short timescale under the original synthetic conditions. In order to resolve the growth kinetics, we tried to gradually add the Se anion precursors in multiple times so that the growth rate could be slowed down. We found that the formation of QDs include two steps – the nuclei formation and the subsequent QD growth. The nucleation is initiated when a small amount of Se anion precursors (0.04 mM) is added into the protein-metal ion complex solution which results in an absorption onset at ~500 nm (Figure S25a). TEM images show the formation of small nuclei with an average diameter of 1.6 ± 0.4 nm (Figure S26a). As more Se precursors were added the absorption spectra gradually shifted to longer wavelength as a result of QD growth (Figure S25a). We found that the protein-metal ion complex formation is critical for the controlled QD seeding and growth. In the absence of protein molecules the QD precursors immediately reacted and precipitated in an uncontrollable manner that leads to the formation of large insoluble aggregates. No soluble products were detected in the absence of BSA (Figure S25b). Taken together, we conclude that the protein-directed QD synthesis undergoes the following mechanism: protein molecules first bind to metal ions to form a complex; this complex facilitates controlled nucleation following the introduction of anion precursors; the as-formed nuclei grow bigger to form QDs by reacting with the free precursors in solution; the protein passivates on QD surface once the QD is formed.

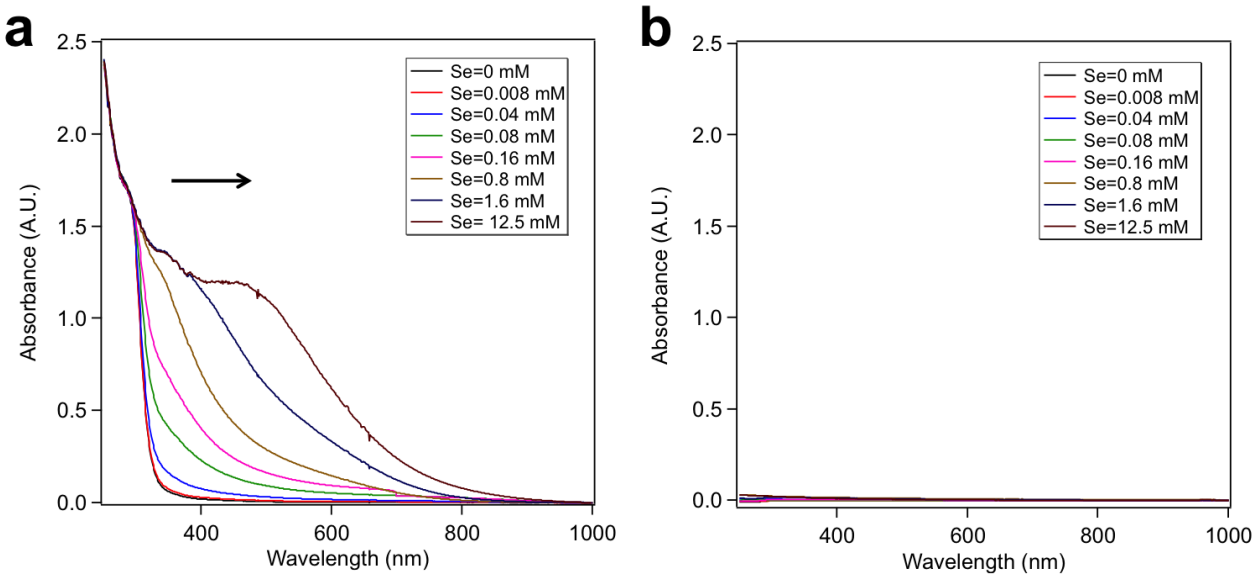

Figure S27. (a) Absorption spectra of the reaction mixture during the course of QDs formation in the presence of BSA. Se precursors were gradually introduced into the reaction mixture in multiple times in order to slow down the growth rate. (b) Absorption spectra of the reaction mixture in the absence of BSA. No soluble products were detected since the QD precursors immediately reacted and precipitated in an uncontrollable manner that leads to the formation of large insoluble aggregates in the absence of BSA.

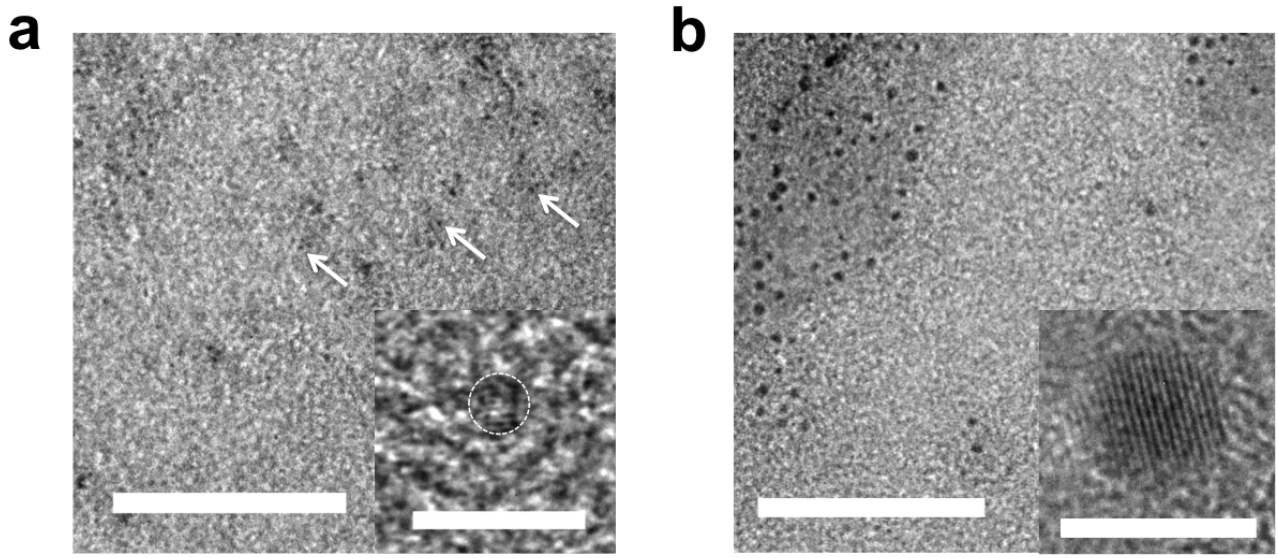

Figure S28. Low magnification and high resolution (insets) TEM images of nuclei (a) and QDs (b) formed in the presence of BSA. (Typical nuclei are indicated by white arrows in (a). The white dashed circle in inset of (a) depicts a single nucleus.) The nuclei in (a) were generated with 0.04 mM Se precursors. The final QDs product in (b) was generated with a total of 12.5 mM Se precursors. (Scale bars are 50 nm in (a) and (b) and 5 nm in insets of (a) and (b))